Available online at www.sciencedirect.com
SCIENCE DIRECT
Surface & Coatings Technology 200 (2006) 3254 – 3260
SURFACE & COATINGS TECHNOLOGY
www.elsevier.com/locate/surfcoat

Combined optical, surface and nuclear microscopic assessment of porous silicon formed in HF-acetonitrile

Z.C. Feng [a,*], J.W. Yu [a], K. Li [b], Y.P. Feng [c], K.R. Padmanabhan [d], T.R. Yang [e]

[a] Graduate Institute of Electro-Optical Engineering and Department of Electrical Engineering, National Taiwan University, Taipei, 106-17 Taiwan, ROC
[b] Chartered Semiconductor Manufacturing Ltd., 60 Woodlands, Industrial Park D, Street 2, Singapore 738406, Singapore
[c] Department of Physics, National University of Singapore, S0511, Singapore
[d] Department of Physics and Astronomy, Wayne State University, Detroit, MI 48201, USA
[e] Department of Physics, National Taiwan Normal University, Taipei, 116 Taiwan, ROC

Available online 31 August 2005

Abstract

A new type of HF solution, HF-acetonitrile (MeCN), has been employed to produce 10–30 μm thick porous silicon (P-Si) layers by photoelectrochemical etching of different types of Si wafers, Si(100), Si(111) and polycrystalline Si, with different resistivities. A combined optical, surface and nuclear microscopic assessment of these P-Si layers was performed using photoluminescence (PL), Raman scattering, X-ray photoelectron spectroscopy and Rutherford backscattering spectroscopy. With increasing resistivity of the Si(100) wafers, the P-Si layers show a slight blue shift of their visible light emission peak energy, an up shift of the peak position and a narrowing of the band width of the dominant Raman band, and a decrease in the amount of residual elemental Si on the surface. Those Si(111) wafers, etched in HF-MeCN, showed no porous structures and no visible light emission.

Keywords: Porous silicon; PL; Raman; RBS; SEM; Raman scattering; XPS

1. Introduction

The observations of the blue shift of the absorption edge [1] and the visible photoluminescence (PL) at room temperature (RT) [2] from porous silicon (P-Si) in the 1990s have attracted world-wide attention to P-Si and related materials [3–6]. These developments have led to the publication of a large number of reports and papers in various journals and conference proceedings [3–5] as well as review books [6–8]. After entering into the 21 century until current days, research on porous Si has been still very active [9–15]. Traditionally, Si is the dominant material for modern electronics and computers. But, its indirect band gap, which lies in the near infrared (NIR), and low light emission quantum efficiency had limited its use in visible optoelectronics. The recent developments in porous Si may, however, fortunately result in the use of the material in visible optoelectronics by merger of its optoelectronic properties and Si-based integrated processing techniques. This may open a new field of processed optoelectronic Si microelectronic devices.

Porous Si can be formed easily by electrochemical etching of single crystalline Si in HF solutions containing electrolytes. The porous Si structures generate visible photoluminescent or electroluminescent light. Many authors [1,2] believe that quantum size effects, based upon the free standing quantum wire model, is the major reason for visible light emission, although several other mechanisms have also been proposed to explain the behavior of RT visible light emissions from P-Si, such as siloxene [16], oxidized Si [17], hydride complexes [18], and an amorphous phase of Si or its complexes [19]. We have used a combination of several sophisticated techniques to understand and distinguish different luminescent mechanisms [20–22].

Porous Si was indeed first described nearly half a century ago [23] and used as the anti-reflectance (AR) layer for solar

* Corresponding author. Tel.: +886 2 3366 3543; fax: +886 2 2363 7467.
E-mail address: zcfeng@ee.cc.ntu.edu.tw (Z.C. Feng).

0257-8972/$ - see front matter © 2005 Elsevier B.V. All rights reserved.
doi:10.1016/j.surfcoat.2005.07.025

cells [24]. Recently, applications of porous Si in photovoltaics have been explored [25–31]. It has been observed that the porous Si layer may greatly decrease the reflectance than the bared Si wafer and thus decrease the optical loss in solar cell structures [26–28,30,31]. Menna et al. [31] studied the reflectance variations with changing the concentration of the oxidizing species and etching times on AR coating P-Si on polycrystalline Si, and concluded that the reduction of the optical losses is affected by the process parameters and is almost independent of the starting substrate. Other studies on the P-Si layers for solar cells [24–30] did not study the effects of the Si substrates also.

The ordinary electrochemical etching of Si in aqueous electrolytes leads to the formation and dissolution of oxide intermediates, which causes dissolution limited currents, hydrogen gas evolution and highly branched microporous structures [1]. It has been shown that these effects can be eliminated or reduced by the photoelectrochemical etching of Si in HF-acetonitrile (MeCN) solutions [32]. Unlike the results in aqueous fluoride electrolytes, in acetonitrile no hydrogen gas is generated, no critical current is observed and the dissolution limited current is more than 1.4 A/cm^2 for *p*-type Si [33]. It is worthy to investigate in depth the P-Si layers produced in these solutions and their various properties.

In this study, we prepared P-Si layers by photoelectrochemical etching of Si in HF-acetonitrile (MeCN), which is different from most of the cases reported in the literature. Different types of Si wafers, including single crystalline Si(100), Si(111) and poly-crystalline Si, with different resistivities, were used to fabricate P-Si layers. Photoluminescence (PL), Raman scattering, X-ray photoelectron spectroscopy (XPS) and Rutherford backscattering spectroscopy (RBS) were employed to study their optical, surface, and structural properties. The properties of P-Si layers prepared from this special HF-MeCN solution are found to be a strong function of the Si substrate crystallinity and resistivity.

2. Experiment

2.1. Sample preparation

Four different boron doped *p*-type Si wafers, 2 Ω cm and 0.2 Ω cm Si(100), 0.02 Ω cm Si(111) and 1 Ω cm polycrystalline Si, with thicknesses ranging between 250 and 350 μm, were used for this investigation. Semiconductor purity anhydrous HF and the pure (<5 ppm water) MeCN electrolyte were used in an inert atmosphere dry box with the water and oxygen concentrations maintained below 2 ppm. A three electrode cell was used with a platinum counter and silver reference electrode. The P-Si layers were formed by anodizing Si wafers under the same conditions, e.g. in 2 M HF:0.25 M TBAP (tetrabutylammonium perchlorate) with a current density of 7 mA/cm^2 for 30 min. The porous structures produced by this technique were examined by a Hitachi S-2700 scanning electron microscope (SEM). The thickness of P-Si layers was found to be in the range of 10–30 μm. P-Si samples prepared in (100) Si and poly-Si wafers, showed macro-pores of about 1 to 2 μm in diameter and 10–20 μm in depth [31], associated with the micro-porous structures (<100 nm) [34]. However, unlike the etching of (111) Si in aqueous HF solutions, no pores were found for the Si(111) sample etched in HF-MeCN [33]. More details on the P-Si preparation by using these special HF-MeCN solutions were given in Refs. [20,21].

2.2. Assessment techniques

Room temperature (RT) PL measurements were performed, using a SPEX-1404 system with a laser excitation of 4880 Å (50 mW) from a Ar^+ ion laser. Spectral reflectance was measured at RT in the wavelength range of 400–850 nm with 10 nm per data. Scanning electron microscope (SEM) observation was done using a Philips SEM system. Raman scattering was measured at RT and in the near backscattering geometry. Samples were excited with the 4067 Å line from a 8 W Coherent Kr^+ ion laser. The scattered light was dispersed by a SPEX-1877 triple spectrometer with a resolution of ~3 cm^{-1}, detected and accumulated by an optical multichannel analyzer (OMA) with high signal-to-noise ratio under computer control. XPS was performed using a VG ESCALAB MkII spectrometer with a Mg Kα X-ray source (1253.6 eV, 120 W) at a constant analyzer pass energy of 20 eV. RBS and ion channeling were measured using 2 MeV α-particle beams as the incident source.

3. Results and discussion

3.1. Room temperature photoluminescence

All samples display broad emission bands ranging between 5300 Å and 8700 Å. The central or peak position of the PL bands differs slightly among these samples and is located in the red color region between 6500 and 6800 Å. The PL emission intensities are also varied with the samples. The sample prepared from the 0.2 Ω cm Si(100) wafer possesses the strongest PL emission band, the 2 Ω cm Si(100) sample second and the 1 Ω cm poly-Si third. The 0.02 Ω cm Si(111) sample showed almost no visible light emission, consistent with the SEM observation of no pores. It is suggested that (111) Si oxidation–dissolution occurs through a tetravalent route in HF-MeCN solutions [33], which leads to no pores formed for Si(111) etched in HF-acetonitrile and no RT PL light emission is observed for this sample in Fig. 1.

According to the literature [35–37] the PL peak energy from P-Si exhibits generally a blue shift with increasing the resistivity of Si wafer. It has also been shown [1,37] that

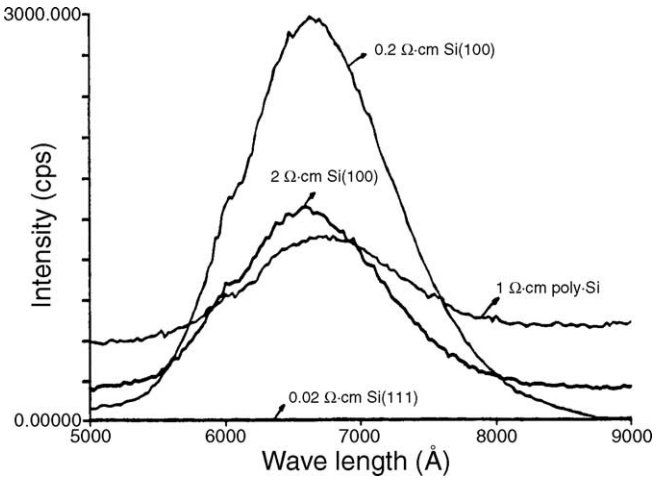

Fig. 1. RT-PL spectra from four porous-Si samples.

increasing the porosity of P-Si may lead to a blue shift of the PL peak energy which has been demonstrated by the quantum size effect. Comparing two PL curves of P-Si prepared from Si(100) wafers in Fig. 1, a slight PL blue shift can be seen as resistivity, ρ, increases from 0.2 Ω cm to 2 Ω cm. However, this trend is not true if we compare the 1 Ω cm poly-Si case with the above two Si(100) wafers. Therefore, the appearance of the blue shift of PL peak energy depends not only on the resistivity but also on crystallinity and other material parameters of Si wafers used to form P-Si. This is also true for the PL intensity comparison of different P-Si layers.

3.2. SEM

Fig. 2 shows two typical SEM photos from P-Si prepared from 2 and 0.2 Ω cm Si(100). It is seen that the pore sizes of the P-Si layer on 2 Ω cm Si(100) are much larger than that of the P-Si layer on 0.2 Ω cm Si(100). This can be explained as follows. As a Si wafer contains more impurities with a low resistivity, the electrochemical etching rate along the normal direction of the surface will be fast but the total amount of the etched masses per unit time may be almost constant. Therefore, the etching rate in plane is less for a low resistivity Si(100) wafer than for a high wafer. Thus, we obtained the pore sizes of P-Si/0.2 Ω cm Si(100) to be less than that of P-Si/2 Ω cm Si(100). The bigger pore structures will make the left Si skeleton with small dimensions in the plane direction, leading to stronger quantum size effect. This is consistent with the above observation of the PL blue shift.

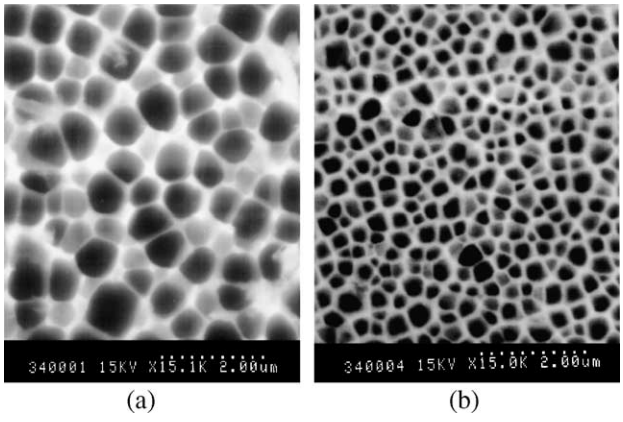

Fig. 2. Two typical SEM photos of porous-Si prepared from (a) 2 Ω·cm and (b) 0.2 Ω·cm Si(100).

3.3. Optical reflectance

Fig. 3 exhibits the optical reflectivity spectra over 400–850 nm for several P-Si samples and a single crystalline Si wafer. The Si wafer possesses high resistivity of 30–50% over this wavelength range. As porous layers were formed, the reflectance is greatly reduced. It can be seen that with an increase of ρ, the reflectivity over the entire wavelength range is reduced. This can be explained with our above SEM observation. Larger pore size structure, as seen from

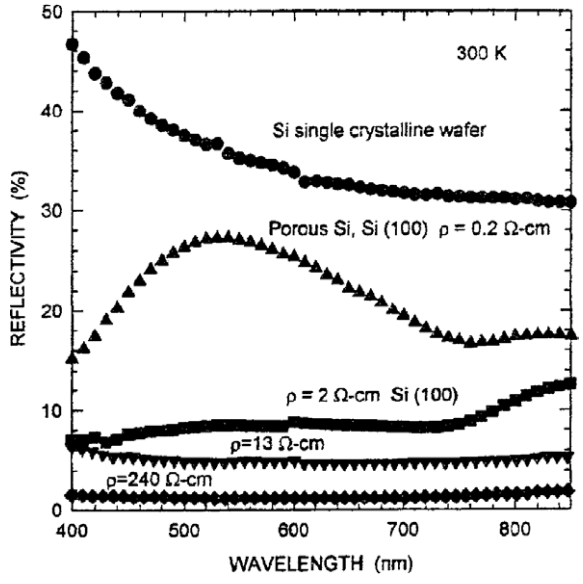

Fig. 3. Optical reflectivity spectra over 400–850 nm for four porous-Si samples and a single crystalline Si wafer.

P-Si prepared on higher ρ Si wafer, will make more incident light to enter into the sample and produce less reflected light, leading to a lower reflectance. But P-Si layers formed from too high ρ wafers, such as 13 and 240 Ω cm Si(100), show no or very weak luminescence. Therefore, we do not discuss these two samples in this study further.

3.4. Raman scattering

Fig. 4 exhibits RT Raman spectra of these four samples under the excitation of 4067 Å at 50 mW. The P-Si sample prepared from a Si(100) wafer with a resistivity of 2 Ω cm displays a Raman band peaked at 520 cm^{-1}. Its band shape is slightly asymmetric with a left half width of 6 cm^{-1} and a right half width of 4 cm^{-1}. This is close to but slightly different from the line shape of the major Raman mode from a crystalline (c-) Si. As decreasing the resistivity from 2 Ω cm to 0.2 Ω cm for Si(100), 0.02 Ω cm for Si(111), and 1 Ω cm for poly-Si, shifts the dominant Raman band downwards, broadens and makes it more asymmetric. The extension of the downshift, broadening and asymmetry increases as decreasing ρ. The shift or variation in Raman line shape characterizes the change in porous Si structures from sample to sample, and is similar to our results on P-Si membranes prepared in ordinary HF solutions [20–22].

3.5. Raman line shape analysis

A theoretical model, named "Spatial Correlation model", has been developed to describe the Raman line shape of disordered crystals. In an ideal crystal translational symmetry leads to plane wave phonon eigenstates. Only phonons

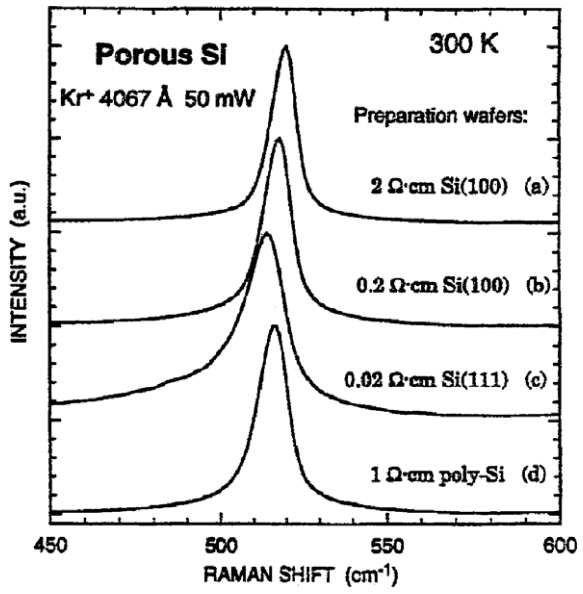

Fig. 4. Room temperature Raman spectra of porous Si prepared from different Si wafers: (a) 2 Ω·cm Si(100), (b) 0.2 Ω·cm Si(100), (c) 0.02 Ω·cm Si(111), and (d) 1 Ω·cm polycrystalline Si.

with $q=0$ at the center of the Brillouin zone (Γ point) are involved in the first-order Raman scattering. The correlation lengths of these phonons are infinite. However, disorder or finite-size effects may completely or partially relax the momentum conservation to have non-zero momentum phonons involved in the first-order Raman process, leading to a downshift and as-symmetric broadening of the Raman peak. The intensity dependence of Raman spectrum on the phonon frequency can be expressed as

$$I(\omega)\alpha\exp\left(-q^2L^2/4\right)d^3q/\left\{[\omega-\omega(q)]^2+(\Gamma/2)^2\right\}, \quad (1)$$

where the correlation length L is in unit of a, the lattice constant, q, is expressed in units of $2\pi/a$, Γ is the natural line-width including the intrinsic width from a non-disordered crystal and the instrumental contributions. The dispersion relation has a form of

$$\omega(q) = A - Bq^2. \quad (2)$$

This spatial correlation model has been employed to analyze the Raman line shape from porous Si. In these work, A and B were used with the values for a crystalline Si with $A=520.5$ cm^{-1} and $B=120$ cm^{-1}. Γ is also setting at a constant value of 3 or 4 cm^{-1}.

In an attempt to use this model to fit our Raman data from porous Si samples, we found that we cannot obtain good fits if we used fixed A, B and Γ. We consider that the phonon dispersions for a crystalline Si and a porous Si might be different because of different structures, and that Γ might differ slightly also because of different measurements, in which we can only set the measurement conditions, including laser beam focusing and optical alignment, as close as possible for different sample measurements, but cannot make them exactly same. Therefore, we perform our theoretical fits including to vary A, B and Γ slightly. The following theoretical formula is used:

$$I(\omega) = I_o q^2\exp\left(-q^2L^2/4\right)\mathrm{d}q/\left\{\left[\omega-A+Bq^2\right]^2 + (\Gamma/2)^2\right\} + I_{bk}, \quad (3)$$

where I_o is the adjusted constant intensity and I_{bk} is the background. I_o and I_{bk} can be adjusted also in fits. In this way, we have very good fits between the experimental and theoretical results. Two examples for the porous Si grown on $\rho=2$ Ω cm Si(100) and poly-Si are shown in Fig. 5(a) and (b), respectively. The fitted parameters are listed in Table 1.

3.6. X-ray photoelectron spectroscopy (XPS)

Fig. 6 (left side) shows the XPS wide-scan spectra of the four porous Si samples. In addition to the peaks due to Si (Si 2p and Si 2s), carbon (C 1s) and oxygen (O 1s) were also detected; other elements could not be detected because of the XPS sensitivity limit of 1% (surface

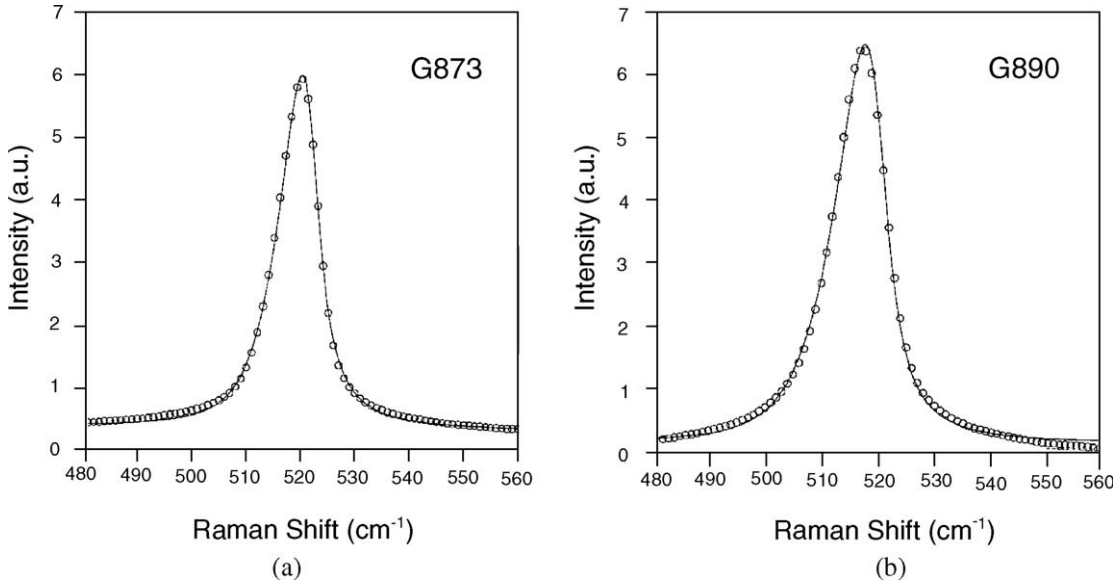

Fig. 5. Raman line shape fits by the spatial correlation model for two porous Si samples: (a) G873, (b) G890.

concentration). There is some variation in relative intensities of the peaks between the four samples. The surface C concentration of the 0.02 Ω cm Si(111) sample is the lowest. This may be due to the relative stability of the dense (111) surface to etching, which may introduce carbon contamination. The Si 2p narrow scans (Fig. 6, right) show that the surfaces of all four samples are largely SiO_2, supporting the strong O 1s peak. The Poly Si spectrum however displays significant amounts of elemental Si at lower binding energy, and to a lesser extent the Si(111) sample as well. This may be explained by the difference in the surface area of poly-Si and c-Si after etching and the subsequent oxidation.

3.7. Rutherford backscattering spectroscopy (RBS)

RBS measurements on these four samples also show the existence of Si, O and C in the porous layers, which is consistent with the XPS results. Moreover, F was detected in very small concentration, which came from the HF solutions. Simulation of RBS data gives the thickness and composition of the P-Si layer for each sample, which shows a large scatter from sample to sample, although they were prepared under the same photoelectric etching conditions. Ion channeling was also done for these samples. Crystalline structural variations between the porous and non-porous regions and from sample to sample were revealed. Fig. 7 shows such an example for the 2 Ω cm Si(100) sample. Random and aligned spectra from porous region, non-porous region and c-Si are exhibited. Different minimum yield ratios were obtained between the aligned and random RBS. Detailed analyses of nuclear data will be given in a future publication.

4. Conclusion

We have prepared porous silicon (P-Si) on various Si substrates by photoelectrochemical etching of silicon in HF-acetonitrile (MeCN) solutions, a new type of HF solutions for forming P-Si. Different types of Si wafers, Si(100), Si(111) and polycrystalline Si, with different resistivities, were employed to produce 10–30 μm thick P-Si layers. A combined optical, surface and nuclear microscopic assessment of these P-Si layers was performed using photoluminescence (PL), Raman scattering, X-ray photoelectron spectroscopy (XPS) and Rutherford backscattering spectroscopy (RBS). Red wavelength PL was emitted from these P-Si samples, prepared from (100) Si and polycrystalline Si, which showed clear porous structures by SEM. The PL

Table 1
Fitting parameters of four porous Si samples

Sample #	Substrate	L (a) (cm^{-1})	L (Å) (cm^{-1})	Γ (cm^{-1})	A (cm^{-1})	B (cm^{-1})	I_o (cm^{-1})	I_{bk} (cm^{-1})
1)	2 Ω cm Si (100)	14.6	79.3	6.0	522.2	116.9	6.03e9	3.67e4
2)	0.2 Ω cm Si (100)	13.2	71.7	6.3	520.8	120.4	2.62e9	1.09e4
3)	0.02 Ω cm Si (100)	9.75	52.9	7.5	519.0	119.8	6.42e8	1.15e4
4)	1 Ω cm poly Si	11.8	64.1	6.0	520.0	117.1	4.16e9	2.01e4

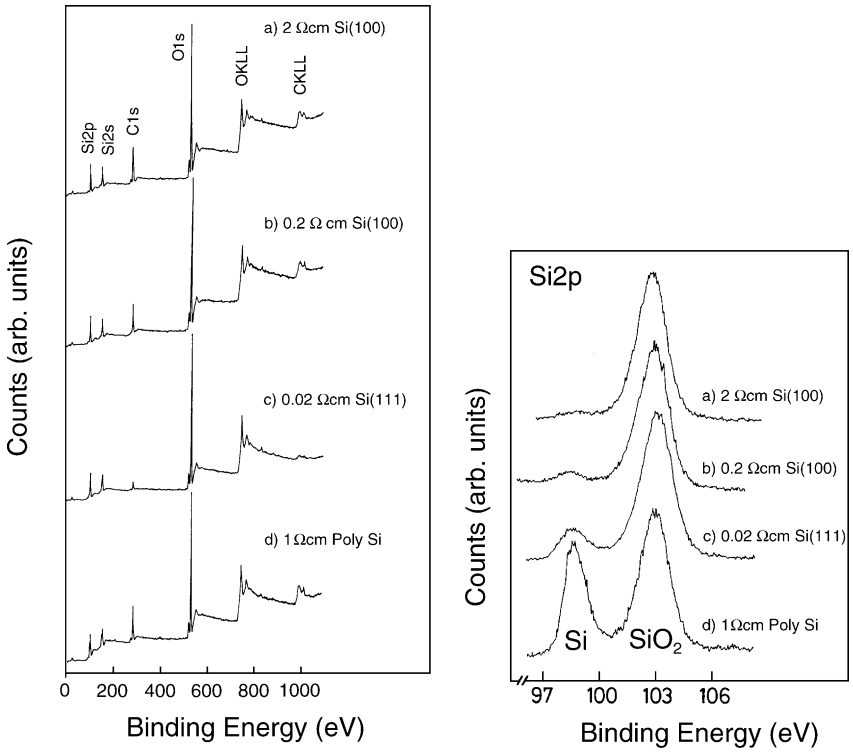

Fig. 6. XPS wide scan spectra of porous Si prepared from different Si wafers: (a) 2 Ω·cm Si(100), (b) 0.2 Ω·cm Si(100), (c) 0.02 Ω·cm Si(111), and (d) 1 Ω·cm polycrystalline Si.

emission intensities are dependent on the properties of Si wafers prepared for forming P-Si. But there is no visible light emitted from samples prepared from (111) Si wafers in which no porous structures were formed. All samples exhibit dominant Raman bands with a slight downshift and a broader/asymmetric shape compared to the c-Si Raman band. The extent of Raman line shape variation is found to be a function of the resistivity of the substrate. XPS studies reveal different surface and oxidation properties from these P-Si layers. Strong C 1s, O 1s, O KLL and C KLL signals together with Si 2s and Si 2p were observed. The amount of contaminant C is varied with ρ. The surfaces of these samples are shown to be largely SiO_2 with different amount of elemental Si, which increases with decreasing ρ of single crystalline Si. P-Si obtained by etching of poly-Si showed the largest amount of elemental Si on the top. RBS data reveal the existence of F on the top in addition to Si, O and C. Simulations of RBS data indicate that there exists a large difference in the thickness and composition of the P-Si layers grown from different wafers. Ion channeling measurements distinguish the crystalline variations between the porous and non-porous regions and from sample to sample. It is worthy to make further investigation on P-Si prepared in HF-MeCN solutions, their luminescence mechanisms and various properties.

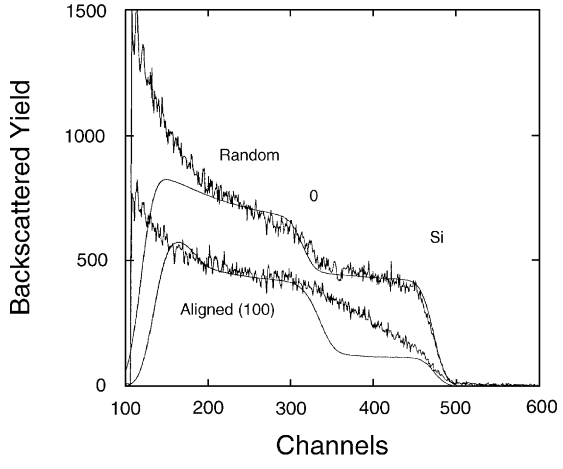

Fig. 7. Random RBS and ion channeling spectra from a porous Si prepared from 0.2 Ω·cm Si(100) wafer (porous and non-porous regions) and simulations (two solid lines, respectively).

Acknowledgement

We acknowledge the help and support from Drs. Z. Chen, A. Rohatgi, A. T. S. Wee, J. Lin, K. T. Yu and S. Perkowitz. The work at National Taiwan University was supported by funds from National Science Council of Republic of China, NSC 93-2218-E-002-011 and 93-2215-E-002-035.

References

[1] V. Lehmann, U. Gösele, Appl. Phys. Lett. 58 (1991) 856.
[2] L.T. Canham, Appl. Phys. Lett. 57 (1990) 1046.
[3] S.S. Iyer, R.T. Collins, L.T. Canham (Eds.), Light Emission from Silicon, Materials Research Society Symposium Proceedings, Materials Research Society, Pittsburgh, 1992.
[4] P.M. Fauchet, C.C. Tsai, L.T. Canham, I. Shimizu, Y. Aoyagi (Eds.), Microcrystalline Semiconductors: Materials Science and Devices, Materials Research Society Symposium Proceedings, Materials Research Society, Pittsburgh, 1993.
[5] M.A. Tischler, R.T. Collins, M.L.W. Thewalt, A. Abstreiter, Silicon Based Optoelectronic Materials, Materials Research Society Symposium ProceedingsMaterials Research Society, Pittsburgh, 1993.
[6] Z.C. Feng, R. Tsu (Eds.), Porous Silicon, World Scientific, Singapore, 1994.
[7] G. Amato, C. Delerue, H.-J. von Bardeleben (Eds.), Structural and Optical Properties of Porous Silicon Nanostructures, Vol. 5 in M.O. Manasreh (Ed.), Optoelectronic Properties of Semiconductors and Superlattices, New York, Gordon and Breach, (1997).
[8] David J. Lockwood (Ed.), Light Emission in Silicon From Physics to Devices, Semiconductors and Semimetals, vol. 49, Academic, San Diego, 1998.
[9] V. Chamard, C. Pichat, G. Dolino, Solid State Commun. 118 (1992) 135.
[10] Han-Su Kim, Eric C. Zouzounis, Ya-Hong Xie, Appl. Phys. Lett. 80 (2002) 2287.
[11] Masato Ohmukai, Hayato Mukai, Yasuo Tsutsumi, Mater. Sci. Eng., B, Solid-State Mater. Adv. Technol. 95 (2002) 287.
[12] Q.W. Chen, D.L. Zhu, C. Zhu, J. Wang, Y.G. Zhang, Appl. Phys. Lett. 82 (2003) 1018.
[13] Ch. Populaire, B. Remaki, V. Lysenko, D. Barbier, Appl. Phys. Lett. 83 (2003) 1370.
[14] L.G. Jacobsohn, B.L. Bennett, D.W. Cooke, R.E. Muenchausen, J. Appl. Phys. 97 (2005) 33528.
[15] T.V. Torchynska, A. Vivas Hernandez, A. Diaz Cano, J. Appl. Phys. 97 (2005) 33507.
[16] M.S. Brandt, H.D. Fuchs, M. Stutzmann, J. Weber, M. Cardona, Solid State Commun. 81 (1992) 307.
[17] Z.Y. Xu, M. Gal, M. Gross, Appl. Phys. Lett. 60 (1992) 1375.
[18] S.M. Prokes, O.J. Glembocki, V.M. Bermudez, R. Kaplan, L.E. Friedersdorf, P.C. Season, Phys. Rev., B 45 (1992) 13788.
[19] R.P. Vasquez, R.W. Fathauer, T. George, A. Ksendzov, T.L. Lin, Appl. Phys. Lett. 60 (1992) 1004.
[20] Z.C. Feng, J.R. Payne, B.C. Covington, Solid State Commun. 86 (1993) 131.
[21] Z.C. Feng, A.T.S. Wee, K.L. Tan, J. Phys., D, Appl. Phys. 27 (1994) 1968.
[22] Z.C. Feng and A.T.S. Wee, in ref. [6], p. 175–194.
[23] A. Uhlir, Bell Syst. Tech. J. 35 (1956) 333.
[24] A. Prasad, S. Balakrishnan, S.K. Jain, G.C. Jain, J. Electrochem. Soc. 129 (1982) 596.
[25] J.P. Zheng, K.L. Jiao, W.P. Shen, W.A. Anderson, H.S. Kwok, Appl. Phys. 61 (1992) 459.
[26] Y.S. Tsuo, Y. Xiao, M.J. Heben, X. Wu, F.J. Pern, S.K. Deb, Proc. 23rd IEEE Photovoltaic Specialists Conf., Louisville, Kentucky, 1993, p. 287.
[27] Y.S. Tsuo, M.J. Heben, X. Wu, Y. Xiao, C.A. Moore, P. Verlinden, S.K. Deb, Mater. Res. Soc. Symp. Proc. 283 (1993) 405.
[28] Y.S. Tsuo and Y. Xiao, in ref. [6], p. 347–362.
[29] G.-P. Wei, Y.-M. Zheng, Z.-J. Huang, Y. Li, J.W. Feng, Y.-W. Mo, Sol. Energy Mater. Sol. Cells 35 (1994) 319.
[30] S.M. Vernon, N.M. Kalkhoran, H.P. Maruska and W.D. Halverson, private communication.
[31] P. Menna, G. Di Francia, V. La Ferrara, Sol. Energy Mater. Sol. Cells 37 (1995) 13.
[32] E.K. Propst, P.A. Kohl, J. Electrochem. Soc. 141 (1994) 1006.
[33] M.M. Rieger, P.A. Kohl, J. Electrochem. Soc. 142 (1995) 1490.
[34] E.K. Propst, M.M. Rieger, K.W. Vogt, P.A. Kohl, J. Electrochem. Soc. 141 (194) L78.
[35] L.E. Friedersdort, P.C. Searson, S.M. Prokes, O.J. Glembocki, J.M. Macaulay, Appl. Phys. Lett. 60 (1992) 2285.
[36] V. Petrova-Koch, T. Muschik, A. Kux, B.K. Meyer, F. Koch, V. Lehmann, Appl. Phys. Lett. 61 (1992) 943.
[37] G.G. Qin, in ref. [6], pp. 195–218.